Sub-5 nm structured films by hydrogen bonded siloxane liquid crystals and block copolymers

Journal of Materials Chemistry C

COMMUNICATION

Sub-5 nm structured films by hydrogen bonded siloxane liquid crystals and block copolymers

Koen Nickmans,[a] Rob C. P. Verpaalen,[a] Jeffrey N. Murphy,[a] Albert P. H. J. Schenning*[ab]

Received 00th January 20xx,
Accepted 00th January 20xx

DOI: 10.1039/x0xx00000x

www.rsc.org/

This paper describes the synthesis and characterization of a novel class of hydrogen-bonding oligo(dimethylsiloxane)-based thermotropic liquid crystals (LCs), with which polymeric supramolecules were obtained with glassy smectic and columnar sub-5 nm features when combined with poly(4-vinylpyrine) homopolymer or poly(sytrene)-b-poly(4-vinylpyridine) block copolymer (BCP). The hierarchical self-assembly afforded by the LC/BCP complexes further resulted in the vertical orientation of the LC features in thin films.

Unlike conventional diblock copolymers (BCPs), the self-assembly of small molecules is not limited by an order-disorder transition at low molecular weight, allowing the formation of sub-5 nm features[1,2] for applications including organic electronics,[3–7] nanoporous membranes,[8–11] and ultra-fine nanolithographic resists.[12–14] In particular, hybrid organic/inorganic small molecules such as those based on polyhedral oligomeric silsesquioxane (POSS)[15,16] or oligo(dimethylsiloxane) (ODMS)[13,17] are advantageous, since their chemical immiscibility leads to phase separation into highly ordered nanostructures and a high etch contrast between molecular components. In principle, these materials could be used to fabricate inorganic nanostructure arrays with sub-5 nm features by etching. However, there are still major challenges concerning this novel class of materials; including control over the self-assembled nanostructured morphology, the formation of defect-free patterns in thin films with a predetermined orientation, and their conversion into functional materials and devices.

We previously reported a series of ODMS liquid crystals (LCs) which form columnar[13] and lamellar[18] morphologies with sub-5 nm dimensions. The high mobility of LC phases makes these materials amenable to directed self-assembly processes for the formation of large-area ordered structures,[10,13,19,20] such as graphoepitaxy,[13] and photoalignment.[21] However, obtaining vertically oriented features remains challenging given the low surface energy of ODMS (γ_{PDMS} ~ 20.4 mN/m).[13,22] Moreover, the low glass transition temperature (T_g) associated with these materials ($T_{g,\ PDMS}$ ~ -127 °C)[23] prevents the 'freezing-in' of metastable structures, and could lead to the deformation of the nanopatterns during processing.[14,24] To address these challenges, it would be desirable to combine the sub-5 nm feature sizes of hybrid organic/inorganic small molecules with the properties and processing of glassy polymeric materials.

Glassy polymeric supramolecular assemblies (PSA) have been constructed through the linking of small molecules to polymer side chains *via* noncovalent interactions such as hydrogen bonding, electrostatic interactions, or metal ligation.[25–33] The main advantage of PSAs is that they enable morphological control through a modular mixing approach,[34–36] as opposed to cumbersome organic synthesis. Extensive studies have been carried out on PSA systems consisting of n-alkylphenols in combination with poly(4-vinylpyrine) (P4VP) [37,38] or poly(styrene)-b-poly(4-vinylpyrine) (PS-b-P4VP).[35,39,40] Early work by the group of Ikkala[28,29,35] showed that pentadecylphenol (PDP) can form a smectic (Sm) LC phase in the microdomains of PS-b-P4VP. A key aspect of the hierarchical self-assembly is that the BCP features are oriented perpendicular to those formed by PDP on a smaller length scale.[35] Since this pioneering work, other small molecules have been combined with P4VP to form PSA materials with more complex morphologies,[41,42] and specific functionalities,[39] such as perfluorocarbons,[43] oligo(thiophenes),[44] and azobenzenes.[45–49] However, hybrid organic/inorganic PSAs with sub-5nm features have not been reported. Moreover, while most studies have been limited to bulk phase behaviour, the phenomenon of hierarchical self-assembly provides opportunities for controlling the thin film orientation of features,[50] which is important for nanofabrication.

[a] *Laboratory of Functional Organic Materials and Devices, Department of Chemical Engineering and Chemistry, Eindhoven University of Technology, P.O. Box 513, 5600 MB, Eindhoven, The Netherlands*
[b] *Institute for Complex Molecular Systems, Eindhoven University of Technology, 5600 MB, Eindhoven, The Netherlands*
[c] *Electronic Supplementary Information (ESI) available: Materials and Methods, Synthetic Produces and Characterization, Fig S1-S9.*

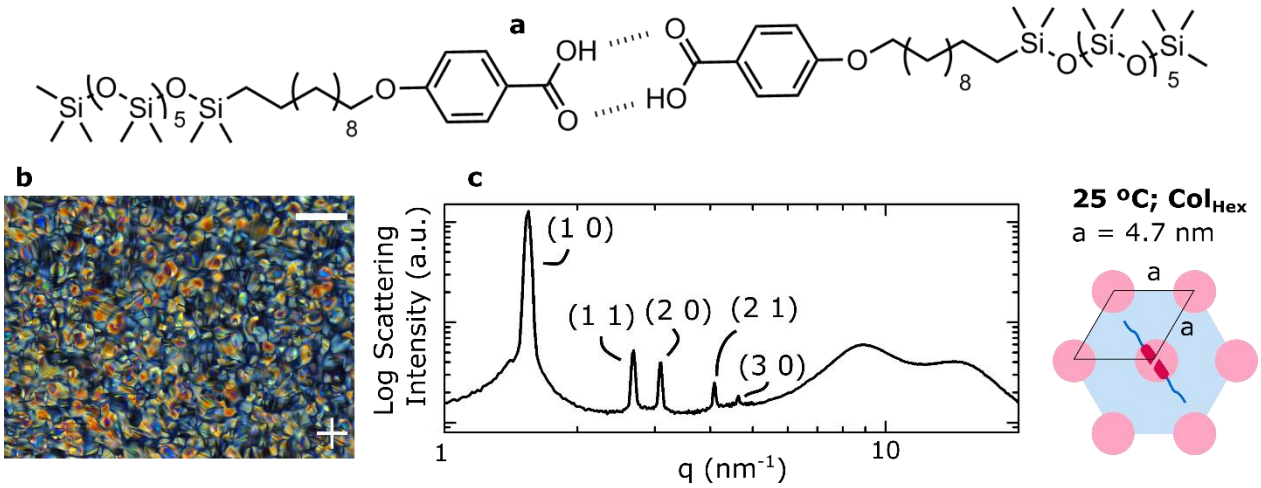

Fig 1. a) Chemical structure of hydrogen bonding ODMS liquid crystal **LC**. b) POM image of **LC** obtained under crossed polarizers at room temperature. The polarizer axes are with a cross. Scale bar: 50 µm c) Bulk x-ray diffraction data of **LC**, collected in both wide- and medium-angle configurations, and concatenated at q = 5 nm^{-1}. The assigned Miller indices and the respective intermolecular scatterings are indicated, as well as a schematic representation of the fitted LC lattice. Hydrogen bonding core = red. ODMS tail = blue. Col_{Hex} = columnar hexagonal.

In this contribution, we report glassy ODMS-based PSAs which are obtained by the hydrogen bonding of an ODMS LC with P4VP and PS-b-P4VP. First, the synthesis and characterization of the novel ODMS LC is discussed, followed by the hierarchical self-assembly behaviour. By adjusting the molar fraction of the LCs within the PSA, smectic and columnar hexagonal morphologies were obtained with sub-5 nm features. The ultra-fine features were oriented vertically in thin films by using the hierarchical self-assembly approach.

Hydrogen bonding ODMS liquid crystal **LC** (Fig 1a) was prepared and fully characterized (Supporting information). According to temperature dependent polarized optical microscopy (POM) (Fig 1b) and differential scanning calorimetry (DSC) (Fig S1), **LC** exhibits a room-temperature (RT) mesophase, marked by the occurrence of birefringent multidomains (Fig 1b). Using bulk X-ray diffraction (XRD) (Fig 1c), two broad peaks were observed in the wide-angle region (6 nm^{-1} < q > 20 nm^{-1}), signifying nano-phase separation between the ODMS (q = 9 nm^{-1}, d = 0.70 nm) and organic (q = 13.4 nm^{-1}, d = 0.45 nm) molecular components. The medium angle reflections (1 nm^{-1} < q > 6 nm^{-1}) were used to assign a hexagonal columnar phase (Col_{Hex}) (plane group p6mm), with a lattice constant of a = 4.69 nm. The formation of a columnar phase as opposed to a smectic phase is likely a consequence of the large coil-to-rod volume fraction due to the bulky ODMS.[51,52] Moreover, since the lattice constant is approximately equal to double the molecular length, (as determined by molecular simulation) the presence of the LC phase is likely driven by dimer formation (Fig 1a).

Initial hydrogen bonding experiments, performed by mixing **LC** with **$P4VP_{15k}$** (PDI=1.25), indicated that hydrogen bonded complexes are readily formed up to high loadings (Fig S2, Fig S3). The resulting PSAs exhibit grainy birefringent textures (Fig S4) and T_g's of approximately 80 °C, considerably lower than that of neat **P4VP** (T_g ~132 °C) [23] (Fig S5). On the basis of these initial experiments, **LC** was mixed with **PS_{33k}-b-$P4VP_{8k}$** (f_{PS} ~ 0.8) (PDI=1.06), to prepare hierarchical PSAs by selective hydrogen bonding of **LC** via the P4VP block (Fig 2a). Hierarchical PSAs were prepared with molar ratios *x* = 0.3, *x* = 0.4, and *x* = 0.5, where *x* = **LC: PS_{33k}-b-$P4VP_{8k}$**. Neat **PS_{33k}-b-$P4VP_{8k}$** exhibits a hexagonal (HEX) morphology in bulk (P4VP minority phase), but is expected to form a lamellar (LAM) morphology upon addition of **LC**, by the increase of volume fraction of the combined **$P4VP_{8k}(LC)_x$** block.[40] The hierarchical PSAs exhibit comparable hydrogen-bonding behaviour and thermal transitions compared to the homopolymer system, with the exception of an additional glass transition at 120 °C, which corresponds to the **PS_{33k}** domains.[23] The presence of distinct glass transition temperatures for **PS_{33k}** (95 °C) and **$P4VP_{8k}(LC)_x$** (80 °C) already indicates the immiscibility of the blocks.

The **PS_{33k}-b-$P4VP_{8k}(LC)_x$** materials were investigated by bulk XRD. To capture the hierarchical multi-scale self-assembly, scattering data was obtained in small-angle and medium-angle configurations. Fig 2b shows the combined data (concatenated at q = 0.7 nm^{-1}) together with the assigned lattice constants and miller indices. For *x* = 0.3, a smectic-in-lamellar (Sm-in-LAM) phase is observed (d = 37.0 nm, a = 5.81 nm). For *x* = 0.5, a (Col_{Hex}-in-LAM) phase is observed (d = 40.6 nm, a = 6.3 nm) and at the intermediate molar ratio (*x* = 0.4) a combination of medium angle scatterings are observed in addition to the LAM morphology of the BCP, indicating the co-existence of Sm and Col_{Hex} morphologies (mixed-in-LAM). Overall, the lamellar spacing increases slightly with increasing *x*, likely due to the increase in combined molecular weight ($d \propto N^{2/3}$). The Sm to Col_{Hex} transition can be understood by volumetric arguments,[34] and suggests that the vinyl(pyridines) are at the centre of the supramolecular cylinders in the Col_{Hex} phase. 2D XRD plots of shear-aligned samples further indicate the orthogonal nature of the hierarchical self-assembly (Fig S6). In order to visualise the

hierarchical nature of the self-assembly, transmission electron microscopy (TEM) was performed on a **PS$_{33k}$-b-P4VP$_{4k}$(LC)$_{0.5}$** thin film. To this end, thick films were prepared by dropcasting on an epoxy substrate, and solvo-thermal annealed with chloroform to promote ordering. Large area TEM images of different unstained polymer sections reveal the presence of alternating layered structures with high lateral order across the image (Fig S7). Within the layers, smaller features are contained. Analysis of a zoomed-in image (Fig 2c) reveals that the layered structures have a periodicity of *ca.* 35 nm, corresponding to the BCP lattice spacing. Perpendicular to these lamellae, features with a periodicity of ca. 6 nm are observed, corresponding the LC phase of the **P4VP$_{15k}$(LC)$_{0.5}$** component. Interestingly, the morphology at the interface between the PSA and the epoxy substrate (Fig 3d) shows that the PSA is directed at the substrate interface. The BCP lamellae are oriented parallel to the epoxy substrate, and by extension, the LC features are oriented in a perpendicular fashion. Moreover, the interface layer appears to consist of an LC layer.

For nanofabrication purposes, vertically oriented Sm features must be achieved in thin films. In order to investigate the effect of hierarchical PSAs on the thin film orientation of LC features, thin films were prepared by spin-coating dilute solutions of **P4VP$_{15k}$(LC)$_x$** and **PS$_{33k}$-b-P4VP$_{8k}$(LC)$_x$** on Si wafers bearing an antireflective coating. Solutions of 2 wt % in chloroform resulted in *ca.* 80 nm thin films, according to ellipsometry. The cast films where thermally annealed at 85°C for 1h to develop large-area alignment, which was not present in as-cast films (Fig S8). Fig 3 shows the characterization data for Sm PSAs **P4VP$_{15k}$(LC)$_{0.4}$** and **PS$_{33k}$-b-P4VP$_{8k}$(LC)$_{0.3}$**. Fig 3a shows the atomic force microscopy (AFM) height map for **P4VP$_{15k}$(LC)$_{0.4}$** which is marked by the presence of distinct plateaus. According to the cross-section (shown by the black line), the height of the plateaus are *ca.* 6 nm, which corresponds to the smectic layer spacing expected for this material, and indicate the presence of smectic layers which are oriented parallel to the surface. Since the surface energy of the ODMS tails is presumed to be very low (γ_{PDMS} = 20.5 mN/m),[23] the siloxane tails are anticipated to wet the air interface, driving the parallel orientation. In contrast, for **PS$_{33k}$-b-P4VP$_{8k}$(LC)$_{0.3}$**, (Fig 3b) plateaus are observed with a height of *ca.* 37 nm, corresponding to the BCP layer spacing. This finding implies the parallel orientation of BCP features, and by extension, the vertical alignment of LC features inside the film. To investigate the through-film morphology of the annealed films, small-angle grazing-incidence x-ray diffraction (GIXRD) was performed. Fig 3c shows that the scattering data for **P4VP$_{15k}$(LC)$_{0.4}$** can be fitted assuming a smectic phase (a = 6.0 nm) in which the smectic layers are oriented parallel to the surface, in agreement with AFM observations. In contrast, for **PS$_{33k}$-b-P4VP$_{8k}$(LC)$_{0.3}$**, the scattering peaks are oriented parallel to the substrate, indicating that the smectic features are oriented normal to the surface. The absence of diffraction rods originating from the BCP lamellae, indicate indirectly that they are oriented planar to the surface.[50] For the LC cylinders in the Col$_{Hex}$ phase, similar observations are made (Fig S9). Together, these findings indicate that the presence of the **PS** block causes the vertical alignment for both Sm and Col$_{Hex}$ LC features.

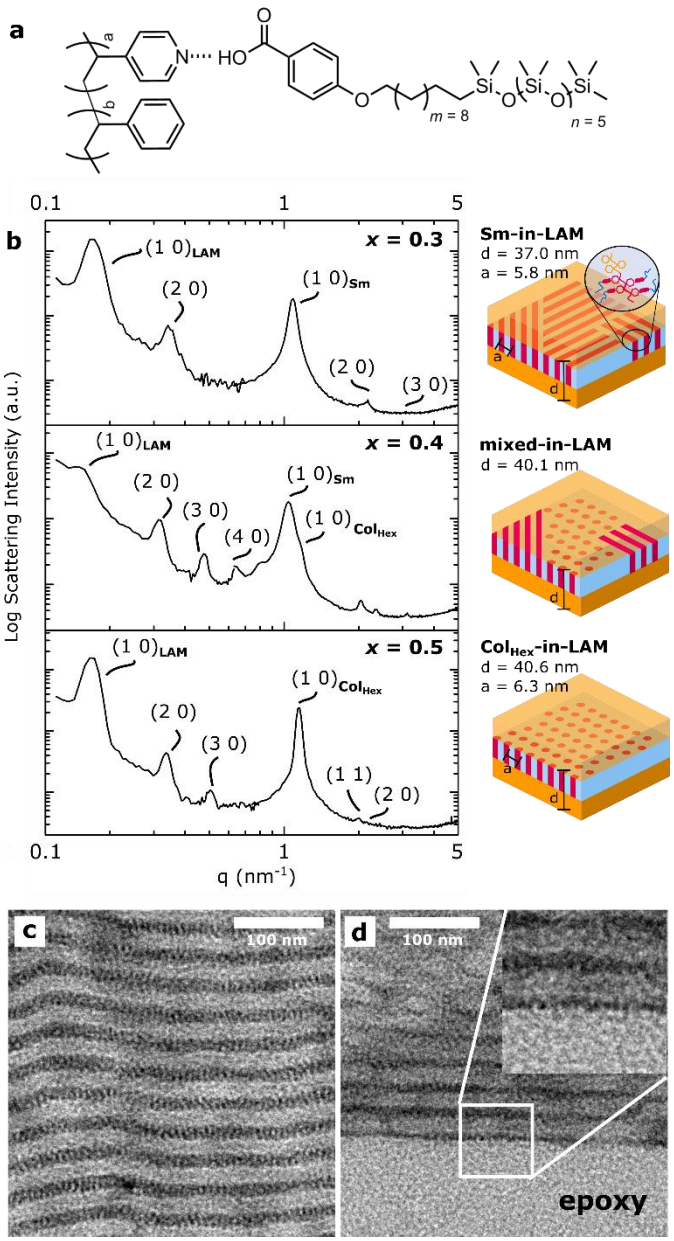

Fig 2. a) Chemical structures of polymeric supramolecular assembly of PS33k-b-P4VP$_{8k}$(LC)x. The carboxylic group on LC associates selectively with the pyridine group on P4VP via hydrogen bonding. b) Bulk x-ray diffraction data of the PS33k-b-P4VP$_{8k}$(LC)$_x$ polymeric supramolecular assemblies. The XRD spectra were collected in the small-angle and medium-angle configuration, and concatenated at q = 0.7 nm-1. The assigned Miller indices and the respective intermolecular scatterings are indicated, as well as the corresponding lattices. P4VP + hydrogen bonding core = red, ODMS tail = blue, PS = yellow. Sm = Smectic. LAM = lamellar, Col$_{Hex}$ = columnar hexagonal. c-d) Transmission electron micrographs of PS33k-b-P4VP4k(LC)0.5 on an epoxy substrate. PS lamellae are light; ODMS side chains are dark. d) TEM image of the PSA at the epoxy interface (inset = 2x magnification).

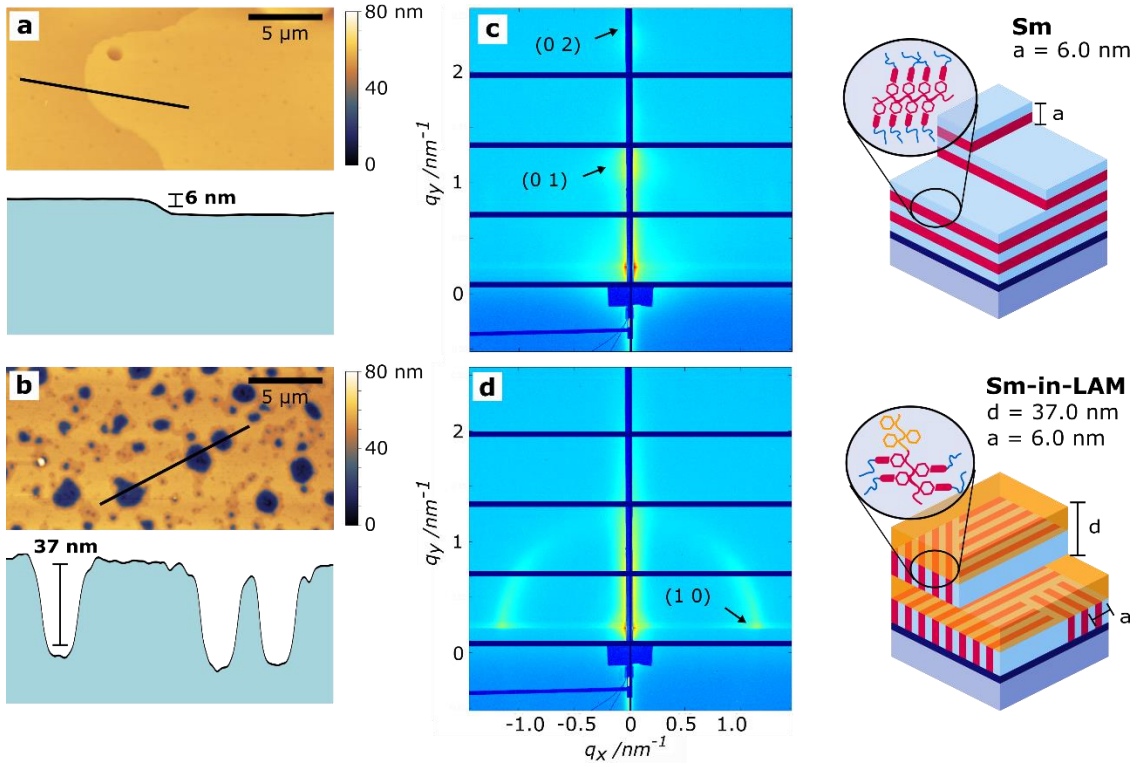

Fig 3. Thin film characterization of PSA thin films of thickness *ca.* 80 nm consisting of **P4VP$_{15k}$(LC)$_{0.4}$** (top) and **PS$_{33k}$-b-P4VP$_{8k}$(LC)$_{0.3}$** (bottom). a-b) Atomic force microscopy height images and associated cross-sections. c-d) Grazing-incidence x-ray diffraction data in small-angle configuration, measured around the critical angle. Schematic representations of the thin film structure from combined GIXRD and AFM observations are shown on the right, as well as the corresponding lattices. P4VP + hydrogen bonding core = red, ODMS tail = blue, PS = yellow. Sm = Smectic. LAM = lamellar.

Conclusions

In conclusion, novel hydrogen bonding ODMS LCs were prepared, characterized, and their thermotropic phase behavior was investigated. The LCs were subsequently mixed with a glassy hydrogen-bond accepting polymer (P4VP) and selectively hydrogen-bond accepting block copolymer (PS-b-P4VP) in various molar ratios. This modular approach results in the formation of a range of glassy nanostructured morphologies in which the phase behavior can be controlled by the mixing ratio. By mixing the LCs with a block copolymer, oriented hierarchical structures were generated, including Sm-in-LAM and Col$_{Hex}$-in-LAM morphologies. The synergistic co-assembly was used to obtain vertical alignment of the sub-5 nm Sm and Col$_{Hex}$ features, which could lead to the fabrication of dense line spaces and contact holes, respectively. In perspective, the sandwiching of the sub-5 nm LC features between PS lamellae to achieve the vertical orientation of low surface energy ODMS, has the potential to eliminate the need for a top-coat (to control surface-air interactions),[53,54] a neutral brush layer at the interface of the substrate, or photoalignment.[21] In order to move towards the utilization of these materials as high etch contrast, glassy, self-assembled resists, monolayer "sandwich" structures must be prepared by adjusting the spin-coating parameters, followed by the removal of the polymeric top layer using dry etching techniques. This work, together with etching and pattern transfer to yield inorganic sub-5 nm features, will be the subject of future investigations.

Conflicts of interest

There are no conflicts to declare.

References

1 K. Nickmans and A. P. H. J. Schenning, *Adv. Mater.*, 2018, 30, 1703713.
2 C. Tschierske, *Angew. Chem.-Int. Ed.*, 2013, **52**, 8828–8878.
3 M. O'Neill and S. M. Kelly, in *Liquid Crystalline Semiconductors*, eds. R. J. Bushby, S. M. Kelly and M. O'Neill, Springer Netherlands, 2013, pp. 247–268.
4 S. Sergeyev, W. Pisula and Y. H. Geerts, *Chem. Soc. Rev.*, 2007, **36**, 1902–1929.
5 M. Kumar and S. Kumar, *Polym. J.*, 2017, **49**, 85–111.
6 Y. Shimizu, in *Nanoscience with Liquid Crystals*, ed. Q. Li, Springer International Publishing, 2014, pp. 257–280.
7 M. O'Neill and S. M. Kelly, in *Liquid Crystalline Semiconductors*, eds. R. J. Bushby, S. M. Kelly and M. O'Neill, Springer Netherlands, 2013, pp. 219–245.
8 C. L. Gonzalez, C. W. M. Bastiaansen, J. Lub, J. Loos, K. Lu, H. J. Wondergem and D. J. Broer, *Adv. Mater.*, 2008, **20**, 1246–1252.
9 M. Zhou, T. J. Kidd, R. D. Noble and D. L. Gin, *Adv. Mater.*, 2005, **17**, 1850–1853.
10 X. D. Feng, M. E. Tousley, M. G. Cowan, B. R. Wiesenauer, S. Nejati, Y. Choo, R. D. Noble, M. Elimelech, D. L. Gin and C. O. Osuji, *ACS Nano*, 2014, **8**, 11977–11986.

11 J. R. Werber, C. O. Osuji and M. Elimelech, *Nat. Rev. Mater.*, 2016, **1**, 16018.
12 S. Hara, H. Wada, A. Shimojima and K. Kuroda, *ACS Nano*, 2017, **11**, 5160–5166.
13 K. Nickmans, J. N. Murphy, B. de Waal, P. Leclère, J. Doise, R. Gronheid, D. J. Broer and A. P. H. J. Schenning, *Adv. Mater.*, 2016, **28**, 10068–10072.
14 K. Nickmans, P. Leclère, J. Lub, D. J. Broer and A. P. H. J. Schenning, *Soft Matter*, 2017, **13**, 4357–4362.
15 Q. Ye, H. Zhou and J. Xu, *Chem. – Asian J.*, 2016, **11**, 1322–1337.
16 X. Yu, K. Yue, I. F. Hsieh, Y. Li, X. H. Dong, C. Liu, Y. Xin, H. F. Wang, A. C. Shi, G. R. Newkome, R. M. Ho, E. Q. Chen, W. B. Zhang and S. Z. Cheng, *Proc Natl Acad Sci U A*, 2013, **110**, 10078–83.
17 R. H. Zha, B. F. de Waal, M. Lutz, A. J. Teunissen and E. W. Meijer, *J. Am. Chem. Soc.*, 2016, **138**, 5693–8.
18 K. Nickmans and A. P. H. J. Schenning, in *Proc. SPIE 10125*, 2017, vol. 10125, p. 1012513.
19 X. Feng, K. Kawabata, G. Kaufman, M. Elimelech and C. O. Osuji, *ACS Nano*, 2017, **11**, 3911–3921.
20 K. Kwon, J. M. Ok, Y. H. Kim, J.-S. Kim, W.-B. Jung, S.-Y. Cho and H.-T. Jung, *Nano Lett.*, 2015, **15**, 7552–7557.
21 K. Nickmans, G. M. Bögels, C. Sánchez-Somolinos, J. N. Murphy, P. Leclère, I. K. Voets and A. P. H. J. Schenning, *Small*, 2017, **13**, 1701043.
22 J. G. Son, K. W. Gotrik and C. A. Ross, *ACS Macro Lett.*, 2012, **1**, 1279–1284.
23 S. Wu, *Polymer Handbook*, Wiley-Interscience, New York, New York, 3rd edn., 1989, vol. VI.
24 K. Lee, M. Kreider, W. Bai, L.-C. Cheng, S. S. Dinachali, K.-H. Tu, T. Huang, K. Ntetsikas, G. Liontos, A. Avgeropoulos and C. A. Ross, *Nanotechnology*, 2016, **27**, 465301.
25 I. Davidi, D. Patra, D. Hermida-Merino, G. Portale, V. M. Rotello, U. Raviv and R. Shenhar, *Macromolecules*, 2014, **47**, 5774–5783.
26 S. Valkama, O. Lehtonen, K. Lappalainen, H. Kosonen, P. Castro, T. Repo, M. Torkkeli, R. Serimaa, G. ten Brinke, M. Leskelä and O. Ikkala, *Macromol. Rapid Commun.*, 2003, **24**, 556–560.
27 S. Valkama, T. Ruotsalainen, A. Nykänen, A. Laiho, H. Kosonen, G. ten Brinke, O. Ikkala and J. Ruokolainen, *Macromolecules*, 2006, **39**, 9327–9336.
28 J. Ruokolainen, R. Makinen, M. Torkkeli, T. Makela, R. Serimaa, G. ten Brinke and O. Ikkala, *Science*, 1998, **280**, 557–560.
29 O. Ikkala and G. ten Brinke, *Science*, 2002, **295**, 2407–2409.
30 O. Ikkala and G. ten Brinke, *Chem. Commun.*, 2004, 2131–2137.
31 M. Faber, A. H. Hofman, E. Polushkin, G. A. van Ekenstein, J. Seitsonen, J. Ruokolainen, K. Loos and G. ten Brinke, *Macromolecules*, 2013, **46**, 500–517.
32 A. H. Hofman, M. Reza, J. Ruokolainen, G. ten Brinke and K. Loos, *Macromolecules*, 2014, **47**, 5913–5925.
33 G. ten Brinke, J. Ruokolainen and O. Ikkala, in *Hydrogen Bonded Polymers*, ed. W. Binder, Springer Berlin Heidelberg, 2007, pp. 113–177.
34 S.-J. Wang, Y.-S. Xu, S. Yang and E.-Q. Chen, *Macromolecules*, 2012, **45**, 8760–8769.
35 J. Ruokolainen, M. Saariaho, O. Ikkala, G. ten Brinke, E. L. Thomas, M. Torkkeli and R. Serimaa, *Macromolecules*, 1999, **32**, 1152–1158.
36 Y. Cai, M. Zheng, Y. Zhu, X.-F. Chen and C. Y. Li, *ACS Macro Lett.*, 2017, **6**, 479–484.
37 T.-Y. Lai, C.-Y. Cheng, W.-Y. Cheng, K.-M. Lee and S.-H. Tung, *Macromolecules*, 2015, **48**, 717–724.
38 A. H. Hofman, Y. Chen, G. ten Brinke and K. Loos, *Macromolecules*, 2015, **48**, 1554–1562.
39 G. T. Brinke and O. Ikkala, *Chem. Rec.*, 2004, **4**, 219–230.
40 B. K. Kuila, E. B. Gowd and M. Stamm, *Macromolecules*, 2010, **43**, 7713–7721.
41 W.-T. Chuang, T.-Y. Lo, Y.-C. Huang, C.-J. Su, U.-S. Jeng, H.-S. Sheu and R.-M. Ho, *Macromolecules*, 2014, **47**, 6047–6054.
42 I. Vukovic, T. P. Voortman, D. H. Merino, G. Portale, P. Hiekkataipale, J. Ruokolainen, G. ten Brinke and K. Loos, *Macromolecules*, 2012, **45**, 3503–3512.
43 R. Bertani, P. Metrangolo, A. Moiana, E. Perez, T. Pilati, G. Resnati, I. Rico-Lattes and A. Sassi, *Adv. Mater.*, 2002, **14**, 1197–1201.
44 B. J. Rancatore, C. E. Mauldin, J. M. J. Fréchet and T. Xu, *Macromolecules*, 2012, **45**, 8292–8299.
45 A. Priimagi, J. Vapaavuori, F. J. Rodriguez, C. F. J. Faul, M. T. Heino, O. Ikkala, M. Kauranen and M. Kaivola, *Chem. Mater.*, 2008, **20**, 6358–6363.
46 J. del Barrio, E. Blasco, C. Toprakcioglu, A. Koutsioubas, O. A. Scherman, L. Oriol and C. Sanchez-Somolinos, *Macromolecules*, 2014, **47**, 897–906.
47 J. del Barrio, E. Blasco, L. Oriol, R. Alcalá and C. Sánchez-Somolinos, *J. Polym. Sci. Part Polym. Chem.*, 2013, **51**, 1716–1725.
48 J. de Wit, G. A. van Ekenstein, E. Polushkin, K. Kvashnina, W. Bras, O. Ikkala and G. ten Brinke, *Macromolecules*, 2008, **41**, 4200–4204.
49 M. Poutanen, O. Ikkala and A. Priimagi, *Macromolecules*, 2016, **49**, 4095–4101.
50 S. H. Tung, N. C. Kalarickal, J. W. Mays and T. Xu, *Macromolecules*, 2008, **41**, 6453–6462.
51 M. Lee, B. K. Cho, H. Kim, J. Y. Yoon and W. C. Zin, *J. Am. Chem. Soc.*, 1998, **120**, 9168–9179.
52 E. Nishikawa and E. T. Samulski, *Liq. Cryst.*, 2000, **27**, 1457–1462.
53 C. M. Bates, T. Seshimo, M. J. Maher, W. J. Durand, J. D. Cushen, L. M. Dean, G. Blachut, C. J. Ellison and C. G. Willson, *Science*, 2012, **338**, 775–779.
54 H. S. Suh, D. H. Kim, P. Moni, S. Xiong, L. E. Ocola, N. J. Zaluzec, K. K. Gleason and P. F. Nealey, *Nat Nano*, 2017, **12**, 575–581.